Size dependence of the stability, electronic structure, and optical properties of silicon nanocrystals with various surface impurities

V. Kocevski, O. Eriksson, and J. Rusz
Department of Physics and Astronomy, Uppsala University, Box 516, S-751 20 Uppsala, Sweden
(Received 22 December 2014; revised manuscript received 18 February 2015; published 3 March 2015)

We present a comprehensive, ground-state density functional theory study of the size dependence of the optical and electronic properties and the stability of spherical silicon nanocrystals (NCs) with different impurities on the surface. We vary the size of the NCs from 1.0 to 3.5 nm, considering single-bonded (CH_3, F, Cl, OH) and double-bonded (O, S) impurities and bridged oxygen. We show that the density of states (DOS) and absorption indices of the NCs with single-bonded impurities are very similar to each other and the fully hydrogenated NCs, except for the 1.0-nm NCs, where a slight difference is present. In the case of the NCs with double-bonded impurities, the DOS and absorption indices exhibit a significant difference, compared to the fully hydrogenated NCs, for sizes up to 2.5 nm. We argue that this difference arises from the difference in the contribution from the impurity to the states around the gap, which can considerably change the character of the states. We demonstrate that the double-bonded impurities contribute significantly to the states around the gap, compared to the single-bonded impurities, causing changes in the symmetry of these states. This observation was further supported by analyzing the changes of the Fourier transform of the charge densities of the highest occupied and lowest unoccupied eigenstate. We also show that the formation energies of NCs with bridged oxygen and fluorine are the lowest, regardless of the size. Furthermore, we show that high hydrogen concentration can be used to suppress the addition of oxygen and fluorine on the surface of the Si NCs.

DOI: 10.1103/PhysRevB.91.125402 PACS number(s): 73.22.−f, 78.67.Hc, 42.70.Qs, 61.46.Hk

I. INTRODUCTION

Although bulk silicon has been used in many light-absorbing applications for decades, the existence of an indirect band gap, and hence the necessity of coupling of photon emission with a phonon, makes bulk silicon a very inefficient light emitter. This property of bulk silicon can be greatly influenced by making nanocrystals (NCs) [1], where it has been shown that the wave function (WF) of the lowest unoccupied eigenstate (LUMO) becomes more localized around the Γ point, attaining a similar character to the WF of the highest occupied eigenstate (HOMO) [2–4]. This change in the character of the LUMO WF increases the probability of direct transitions from the LUMO to the HOMO level, largely enhancing the photoluminescence (PL) efficiency of Si NCs [5–7], compared to that of bulk Si. Moreover, due to the quantum confinement effect, the band gap in the Si NCs widens with decreasing size, allowing for the band gap to be tailored according to the specific needs. The increased PL efficiency and the tunable band of the Si NCs has been realized in many different applications, from lasers [8,9], light-emitting diodes [10–13], and other optical devices [14–16], to sensors [17–21] and photovoltaics [22–25]. Because of the biocompatibility and nontoxicity, the Si NCs are furthermore becoming one of the leading materials for biological fluorescent imaging [26–31].

However, when left under ambient conditions, the hydrogenated Si NCs are extremely prone to surface oxidation. This surface oxidation considerably changes the PL properties by inducing localized defect states within the gap and redshifting the emitted light [32–37]. Moreover, the localized midgap states and the trapping of the exciton at the Si=O bond [33] give rise to PL with very similar energy, when the size of the NCs is less than ∼3 nm [33,38–41]. In many applications, Si NCs that emit light in a particular spectral range are needed; thus, it is necessary to suppress the oxidation of the NCs. To reduce the surface oxidation, the Si NCs' surfaces are passivated with organic molecules [27,42,43], which can greatly improve the PL properties of the NCs. Also, on the surface of the Si NCs there can be other surface impurities, coming as residues from the specific chemicals used in the synthesis of the NCs. Therefore, it is important to have an understanding of the changes in the electronic and optical properties of the Si NCs induced by the addition of various types of surface impurities.

In the past, the dependence of the electronic and optical properties of hydrogenated Si NCs on the size of the NCs, has been extensively studied, employing various theoretical methods; see Refs. [2–4,32,33,44–55], to name a few. However, there have been only a limited number of theoretical studies concerning the size dependence of the electronic and optical properties of Si NCs with different surface impurities [4,33–35,52–58]. A number of these articles focus on the influence of only one surface impurity [33,34,52,54,55], while in others, the Si NCs with partially passivated or fully passivated surface with impurities are studied [4,35,53,56–58]. Among these works, there have been only a few studies of the effect of the surface impurities on the electronic and optical properties for Si NCs larger than 2 nm [4,33,55]. Based on their calculations, Vasiliev *et al.* [34] estimated that the effect of the oxygen on the states around the gap should be present for NCs with size ∼2–2.5 nm, and Wolkin *et al.* [33] showed that the electron can be trapped in oxidized NCs smaller than ∼3 nm. This motivated us to perform a more detailed theoretical study of the size dependence of the electronic and optical properties of Si NCs with surface impurities, where NCs larger than 2 nm are also considered.

Here we present a first-principles study, where Si NCs with size up to 3.5 nm are considered, with various single-bonded and double-bonded impurities, assuming only one impurity

located the surface. We use the ground-state density functional theory (DFT) to calculate the density of states (DOS) and the absorption indices of the studied NCs. From there we extract the HOMO-LUMO gap and the optical absorption gap, and we follow the changes of both gaps with size of the NCs and the type of impurity. We also calculate the projected DOS, to have an overview of the changes in the contribution from the surface impurities, to the states around the gap. We complement these findings by looking into the size evolution of the Fourier transform of the charge densities of the HOMO and LUMO. In addition, we investigate the stability of the NCs, depending on the surface impurity and the size and the changes in the stability with increasing concentration of the impurity.

This paper is structured as follows. In Sec. II we introduce the used surface impurities and the methodology employed in this study. In Sec. III we demonstrate the stability of the Si NCs with different surface impurities, as a function of the NC size, and the dependence of the stability of the NCs on the impurity concentration. In Sec. IV we discuss in details the size dependence of the HOMO-LUMO gap and the optical absorption gap, as well as the DOS and absorption indices. In Sec. V we investigate the contribution from the different impurities to the states around the gap, and the changes that these impurities induce to the HOMO and LUMO WFs, in real and reciprocal space. Finally, in Sec. VI we summarize the concluding remarks.

II. STRUCTURAL MODELS AND METHODOLOGY

To follow the size evolution of the electronic and optical properties of the Si NCs with surface impurities, we consider fully hydrogenated Si NCs, with diameters from 1.0 to 3.5 nm. On the surface of these NCs we inserted various impurities having distinct properties and different types of bonding with the surface Si atoms. We considered a methyl group ($-CH_3$) as a representative of the most common way of passivating the Si NCs and two highly electronegative elements, F and Cl, as impurities. Furthermore, to understand the changes in the properties with the changes in the bonding between the Si atom and the impurity atom, we have considered two types of double-bonded impurities, =O and =S. Because the performance of the Si NCs can be greatly affected by surface oxidation, we also took into account other forms in which oxygen can be bonded on the surface-hydroxyl group (–OH) and bridged oxygen ($-O-$). At the end, we have Si NCs with four different types of single-bonded (SB) impurities ($-CH_3$, $-F$, $-Cl$, $-OH$), two different types of double-bonded (DB) impurities (=O, =S), and bridged oxygen.

For the purpose of our study, we have used the DFT as implemented in the pseudopotential package SIESTA [59], employing local density approximation (LDA) exchange correlation potential. The integration is performed in a real-space three-dimensional (3D) grid, the fineness of which is determined by the plane-wave cutoff. We used a plane-wave cutoff of 160 Ry, the same cutoff as in our previous calculations [3]. Numerical atomic orbitals are used as a basis set, single ζ with polarization orbital (SZP) for Si, double ζ (DZ) for H, and SZP for each of the other considered elements (O, C, F, Cl, S). We refer the reader to Ref. [3] for a more detailed discussion of basis sets for different elements. Furthermore, we explicitly evaluated the dipole transition matrix elements between each occupied and unoccupied eigenstate up to 15 eV, from where the imaginary part of the dielectric tensor is calculated. We used Gaussian broadening of 0.1 when performing the calculations. By employing the Kramers-Kröning transformation of the imaginary part of the dielectric tensor $[\epsilon_{\alpha\alpha}(\omega)]$, we obtained the real part $[\mathrm{Re}\epsilon_{\alpha\alpha}(\omega)]$, from where the absorption indices $[k_{\alpha\alpha}(\omega)]$ can be calculated, using the equation

$$k_{\alpha\alpha}(\omega) = \sqrt{\frac{|\epsilon_{\alpha\alpha}(\omega)| - \mathrm{Re}\epsilon_{\alpha\alpha}(\omega)}{2}}.$$

In the previous study we showed that having a spherical shape or a NC made using the Wulff construction has a rather weak effect on the DOS and absorption indices of the Si NCs [3]. Therefore, in this study we consider only spherical silicon NCs with surface impurities, and as a starting model we used already-relaxed, fully hydrogenated spherical Si NCs from Ref. [3]. The SB impurities ($-OH$, $-F$, $-Cl$, $-CH_3$) are inserted by replacing single hydrogen on the surface of the NC. In the remaining cases, two hydrogens, bonded at the same Si atom, are replaced with DB impurities (=O, =S), or two neighboring hydrogens, bonded to neighboring Si atoms, are replaced with O to make $-O-$. Finally, all of the structures are relaxed until the forces acting on every atom are lower than 0.04 eV/Å. Shown in Fig. 1 are the models of relaxed NCs with oxygen type impurity on the surface.

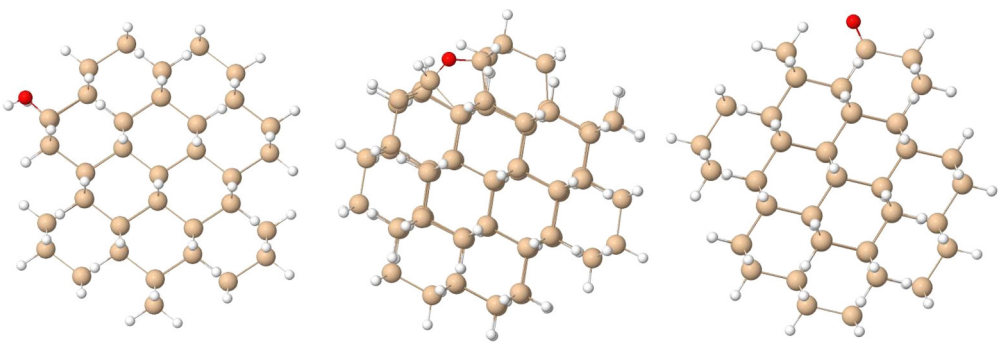

FIG. 1. (Color online) Ball-and-stick models of 1.5-nm Si NCs with (a) $-OH$, (b) $-O-$, and (c) =O. The Si, H, and O atoms are shown in tan, white, and red color, respectively.

III. FORMATION AND GIBBS FREE ENERGY

Despite the great number of experimental, as well as theoretical, studies of Si NCs, there are only few studies concerning the size dependence of the stability of Si NCs with surface impurities [55,60,61]. In order to investigate the stability of the NCs with different surface impurities, depending on the size of the NCs, we calculated the formation energy of the different NCs [$E_f(\mathrm{Si}_N\mathrm{H}_M X)$], per surface area, using the equation

$$E_f(\mathrm{Si}_N\mathrm{H}_M X) = \frac{1}{A}\left[E_{\mathrm{tot}}(\mathrm{Si}_N\mathrm{H}_M X) - N E_{\mathrm{Si}} - \frac{M}{2}E_{\mathrm{H}_2} - E_X\right],$$

where $E_{\mathrm{tot}}(\mathrm{Si}_N\mathrm{H}_M X)$ is the total energy of the NC with relaxed atomic positions and E_{Si} and E_X are the calculated energies per atom for silicon and the impurity, respectively, and E_{H_2} is the calculated energy of an H_2 molecule. The surface area, A (in $\mathrm{\AA}^2$), is calculated as the surface of a convex hull drawn around a bare Si NC. For E_{Si} we used the calculated energy per atom of bulk Si, -107.41 eV, and for E_{H_2} we used the calculated total energy for H_2, -30.55 eV. For the energy of the O, Cl, F, S, CH_3, and OH, we used the calculated values -430.48, -406.06, -645.62, -277.93, -201.50, and -448.04 eV, respectively (see Ref. [62] for more details).

The calculated formation energies for each of the studied NCs, with different types of surface impurities, are shown in Fig. 2. It is noticeable that the $-$O$-$ and $-$F impurities have the biggest effect on the formation energy, significantly decreasing it compared to the other impurities. This shows that the Si NCs with $-$O$-$ and $-$F impurities are the most stable NCs, indicating that inserting this kind of impurity is favorable compared to having only hydrogen passivated surface. This kind of behavior is seen in experiments, where it has been shown that the surface of the Si NCs is easily oxidized and the Si NCs are etched with HF. It is also evident that the formation energies of the 1.0-nm NCs with surface impurities show the biggest difference, compared to the hydrogenated

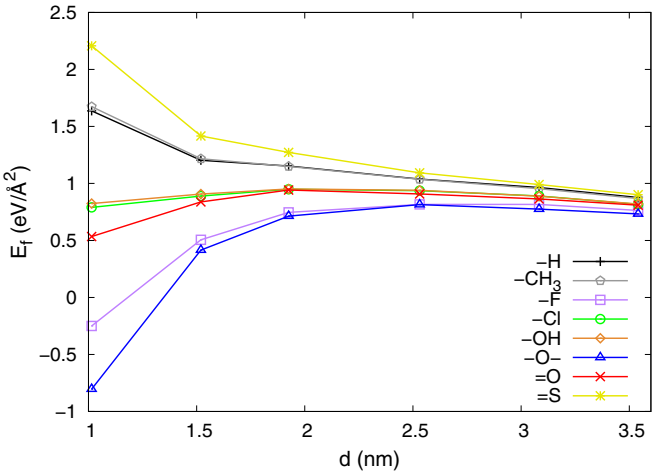

FIG. 2. (Color online) Formation energies per surface area of Si NCs with different types of surface impurities as functions of the size of the NCs. The formation energies of the NCs with $-CH_3$, $-$F, $-$Cl, $-$OH, $-$O$-$, $=$O, and $=$S impurities are shown in gray, purple, green, orange, blue, red, and yellow lines, respectively. The formation energies of fully hydrogenated NCs ($-$H) are shown in black.

NC. The formation energies of the 1.0-nm NCs with $-$O$-$ and $-$F impurity are even negative, indicating that the NCs with these impurities are spontaneously formed at $T = 0$ K. The difference in the formation energies decreases as the NCs size grows, eventually becoming rather small for the 2.5-nm NC. Considering that with increasing NC size the number of Si atoms is growing, the influence of the impurity becomes less pronounced, and the formation energies of the NCs is expected to approach common value. It is also evident that the formation energies of the NCs with SB and DB impurities are distributed over a big energy interval.

Considering that oxygen influences the properties of Si NCs to the greatest extent, and fluorine can be left as a residue after HF etching, it is of interest to investigate the influence of the concentration of oxygen or fluorine, on the stability of the NCs with oxygen or fluorine impurity. Furthermore, it would be instructive to determine at which H_2 concentration the stability of hydrogenated Si NCs is higher than that of the NCs with oxygen or fluorine impurity. Therefore, we calculated the difference between the Gibbs free energies, ΔG of hydrogenated Si NCs, G_{H_2}, and NCs with impurity, G_{X_2} ($X = $ O, F), using the following equation:

$$\Delta G = G_{\mathrm{H}_2} - G_{X_2}.$$

The G_{H_2} and G_{X_2} ($X = $ O, F) are calculated using the equations

$$G_{\mathrm{H}_2} = E_f(\mathrm{Si}_N\mathrm{H}_M) - \frac{\rho_{\mathrm{H}}}{2}\mu_{\mathrm{H}_2},$$

$$G_{X_2} = E_f(\mathrm{Si}_N\mathrm{H}_M X) - \frac{\rho_{\mathrm{X}}}{2}\mu_{X_2}$$

where $E_f(\mathrm{Si}_N\mathrm{H}_M)$ and $E_f(\mathrm{Si}_N\mathrm{H}_M X)$, ($X = $ O, F) are the formation energies, as previously defined, and $\rho_{\mathrm{H}} = \frac{M}{A}$ and $\rho_X = \frac{1}{A}$ are the hydrogen and impurity density at the surface of the NC, respectively. The chemical potential of hydrogen, μ_{H_2}, and of the impurity, μ_{X_2}, at a temperature T and pressure P, is defined as

$$\mu = H^0_{en}(T) - H^0_{en}(0) - T S^0(T) + k_b T \ln\left(\frac{P}{P^0}\right),$$

where S^0 and H_{en} are the entropy and enthalpy at temperature $T = 300$ K, taken from thermochemical tabular data [63], considering the studied species, H_2, O_2, and F_2. P^0 is the reference pressure, set to 1 bar, according to the tabular data, and P and k_b are the partial pressure and the Boltzmann constant, respectively. Shown in Fig. 3 is the evolution of ΔG as a function of the impurity's and hydrogen's chemical potential, where $\mu_{X_2} = \mu_{\mathrm{H}_2}$ ($X = $ O, F).

It is evident that G_{H_2} becomes lower than the G_{X_2} ($X = $ O, F) at high values of the H_2 partial pressure (see the μ_{H_2} values at which ΔG becomes negative in Fig. 3). This indicates that to suppress the addition of oxygen or fluorine on the surface of the hydrogenated Si NCs, a very high H_2 concentration is required. Moreover, comparing the ΔG of Si NCs with $=$O and $-$O- [see Figs. 3(a) and 3(b)], it is noticeable that the ΔG of the NCs with $-$O$-$ impurity becomes negative for higher values of μ_{H_2}, indicating that higher H_2 pressure is required to avoid addition of $-$O$-$ on the surface, compared to the addition of $=$O. Also, to suppress the addition of $-$O$-$ on

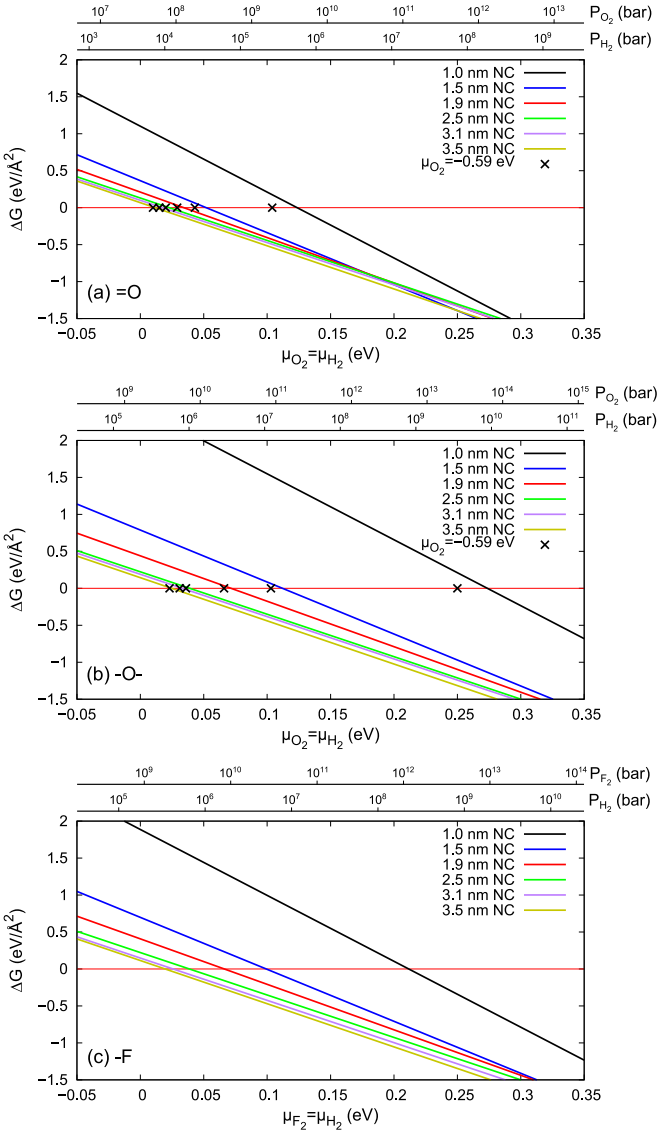

FIG. 3. (Color online) Difference between Gibbs free energies, ΔG, at $T = 300$ K, of hydrogenated Si NCs and Si NCs with (a) $=$O, (b) $-$O$-$, and (c) $-$F impurity. The ΔG is shown as a function of the μ_{H_2} and μ_{X_2}, where $\mu_{X_2} = \mu_{H_2}$. The crosses in (a) and (b) represent the μ_{H_2} value at which ΔG becomes negative, calculated at ambient O_2 pressure, 0.0194 bar ($\mu_{O_2} = -0.59$ eV). The ΔG of NCs with 1.0, 1.5, 1.9, 2.5, 3.1, and 3.5 nm are respectively shown in black, blue, red, green, purple, and yellow.

the surface, a higher H_2 pressure is needed, compared to the addition of $-$F; see Figs. 3(b) and 3(c).

So far we discussed the case where $\mu_{H_2} = \mu_{X_2}$, and to see if lowering the O_2 concentration would considerably lower the H_2 concentration, required to suppress the addition of O on the surface, we consider the O_2 to be at ambient partial pressure, $\sim$0.0194 bar ($\mu_{O_2} = -0.59$ eV). Therefore, first we calculated the G_{O_2} for $\mu_{O_2} = -0.59$ eV, and afterwards we calculated the μ_{H_2} at which $\Delta G = G_{H_2} - G_{O_2} = 0$ eV. These calculated values of μ_{H_2} are shown as crosses in Figs. 3(a) and 3(b). It is evident that even when O_2 is at ambient partial pressure, the H_2 pressure needed to prevent the inclusion of oxygen on the surface of Si NCs is very high for both types of oxygen impurities.

IV. ELECTRONIC AND OPTICAL PROPERTIES

Although there have been studies showing the changes in the DOS of very small Si NCs with surface impurities, depending on the increasing size of the NCs [32,34], for NCs larger than 1.5 nm, these studies only focused on the modification of the DOS [34]. Here we present the DOS of Si NCs with various surface impurities, depending on the size of the NCs, from 1.0 to 3.5 nm; see Fig. 4 for more details.

In the case of SB impurities, $-$F, $-$Cl, $-CH_3$, and $-$OH, the DOS are almost identical to the DOS of hydrogenated NC, regardless of the size. However, there is only one noticeable difference of the DOS of the smallest NC, 1.0 nm, where two small peaks appear as shoulders at the top of the valence band and the bottom of the conduction band. Unlike the bigger NCs, where these states are mainly localized in the center of the NCs, in the 1.0-nm NC, these states display a higher localization around the surface impurity. This was also previously seen for small NCs [32]. These two peaks also appear in the DOS of the 1.0-nm NCs with $-$O$-$, but these are closer to each other, compared to the peaks in the DOS of the NCs with SB impurities. Thus, they are almost detached from the Si states at the top of the valence band and the bottom of the conduction band. On the other hand, the DOS of the NCs with DB impurities, $=$O and $=$S, show much bigger difference compared to the DOS of the hydrogenated NCs. As the size of the NCs is growing, this difference in the DOS becomes less evident, eventually becoming insignificant for the NCs of diameter 3.1 nm or bigger.

Similarly to the DOS of 1.0-nm NCs with SB impurity, in the DOS of the 1.0-nm NCs with DB impurity there are a few small peaks at the top of the valence band and the bottom of the conduction band. However, in the case of the NCs with DB impurity, these peaks are much closer to each other, narrowing the band gap even further. These two peaks can be consistently seen in the DOS of the bigger NC, up to 3.1 nm diameter, where they become absorbed by the conduction and valence bands approaching each other due to reduced effect of the quantum confinement. This is an important observation, because it shows that the effect of a DB impurity on the DOS is becoming negligible for NCs bigger than 3.1 nm.

We further evaluate the influence of the surface impurities on the optical properties of Si NCs with increasing NC size. For that purpose we calculated the absorption indices of the Si NCs with different types of surface impurities, as described in Sec. II, and plotted them as a function of the size of the NCs; see Fig. 5. It is noticeable that the absorption indices of the NCs with SB impurities are very similar to the ones of the hydrogenated NCs with the same size. The only minor difference occurs for the absorption indices of the 1.0-nm NCs, where the first few peaks appear to be more intense in the NCs with surface impurities. This difference can be best seen in Fig. 5(h), where the positive difference between the absorption indices (Δk) of NCs with $-$F impurity and the absorption indices of fully hydrogenated NCs (Ref. [3]) are shown. Similarly to the SB impurities, the $-$O$-$ induces only slight

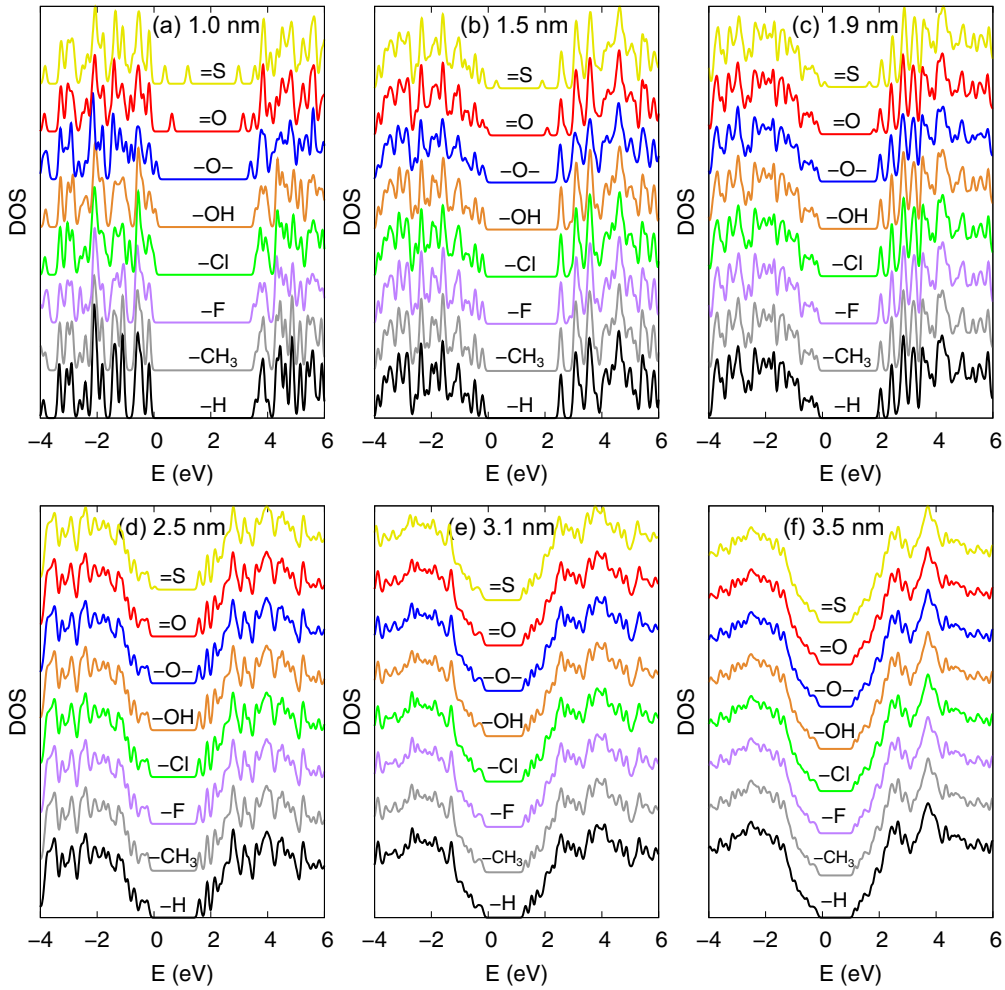

FIG. 4. (Color online) DOS of Si NCs with different surface impurities and size of (a) 1.0 nm, (b) 1.5 nm, (c) 1.9 nm, (d) 2.5 nm, (e) 3.1 nm, and (f) 3.5 nm. For a better view of the midgap states, the DOS are aligned so the most intense peak, at the top of the valence band in each of the NCs, is at the same energy. The DOS of the NCs with $-CH_3$, −F, −Cl, −OH, −O−, =O, and =S impurities are shown in gray, purple, green, orange, blue, red and yellow lines, respectively. The DOS of fully hydrogenated NCs (−H), taken from Ref. [3], are shown in black lines.

change in the absorption index of the 1.0-nm NCs, compared to the absorption index of the fully hydrogenated NC.

Contrary to the NCs with SB impurities, the absorption indices of the NCs with DB impurities exhibit a much bigger change with growing NC size. The most evident difference is in the absorption indices of the 1.0-nm NCs, with both =O and =S impurity, where several peaks emerge below the energy of the first peak in the absorption index of the hydrogenated NC. As the size of the NCs grows, the intensity of the peaks below the energy of the hydrogenated NC decreases, eventually being insignificant for the NCs bigger than 3.1 nm, which is most noticeable in Fig. 5(g). These changes in the absorption indices can be attributed to the decreasing contribution from the surface impurity to the states around the gap and are discussed in more detail later.

For use in many optical applications, from light-emitting to light-absorbing ones, it is very important to know the HOMO-LUMO gap and the optical absorption gap. This becomes even more important when the gaps can be influenced by the surface impurities and the size of the NCs. Therefore, we calculated the HOMO-LUMO gaps and the optical absorption gaps for the Si NCs with different sizes and different surface impurities; see Table I and Fig. 6. The optical absorption gaps are extracted from the absorption indices by considering the lowest energy at which the optical absorption is greater than 0.05. We should point out that the reported gaps are calculated employing ground-state DFT; thus, the values should be considered with care, especially because of the well-known underestimation of the gaps in LDA [64]. For a better comparison with experiments, one should also go beyond the ground-state DFT, considering many-body effects such as the electron-hole interaction or more precise treatments of the electron-electron correlation. For example, in the case of hydrogenated Si NCs GW calculations [47–50], time-dependent DFT [47–49,51] or quantum Monte Carlo [32] can provide a more accurate estimate of the band gaps. However, it has been shown that for hydrogenated Si NCs the ground-state DFT-LDA gives a good estimate of the gaps [3], comparable with experiments and other theoretical approaches. This similarity of the calculated HOMO-LUMO gaps and the experimentally measured optical gaps can be largely attributed to the cancellation of the excitonic and quasiparticle effects [65–67]. In addition, the

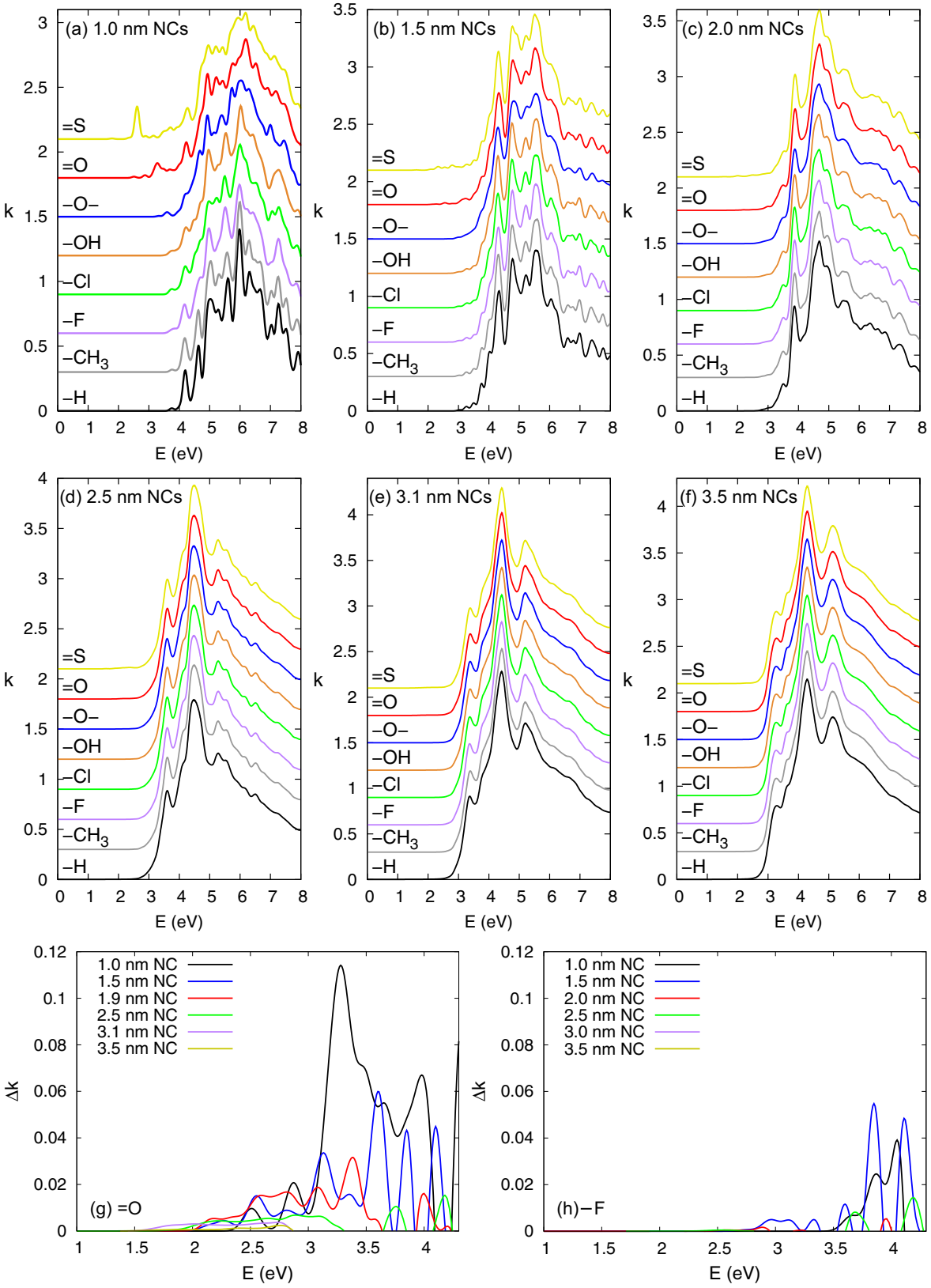

FIG. 5. (Color online) Absorption indices of Si NCs with different surface impurities and sizes of (a) 1.0 nm, (b) 1.5 nm, (c) 1.9 nm, (d) 2.5 nm, (e) 3.1 nm, and (f) 3.5 nm. The absorption indices of the NCs with $-CH_3$, $-F$, $-Cl$, $-OH$, $-O-$, $=O$, and $=S$ impurities are shown in gray, purple, green, orange, blue, red, and yellow lines, respectively. The absorption indices of fully hydrogenated NCs ($-H$), taken from Ref. [3], are shown in black lines. Positive values of the difference between the absorption indices (Δk) of NCs with (g) $=O$ impurity and (h) $-F$ impurity, compared to the absorption indices of the fully hydrogenated NCs (Ref. [3]), as a function of the NC size. Δk of NCs with 1.0, 1.5, 1.9, 2.5, 3.1, and 3.5 nm are respectively shown in black, blue, red, green, purple, and yellow.

TABLE I. Calculated HOMO-LUMO gaps (Fund.) and optical absorption gaps (Opt.) of Si NCs with different diameter (d) and various surface impurities. The gaps are compared to the HOMO-LUMO and optical absorption gaps of fully hydrogenated NC (−H), taken from Ref. [3].

		Type of atomic impurity															
		−H		$-CH_3$		−Cl		−F		−OH		−O−		=O		=S	
Particle[a]	d (nm)	Fund.	Opt.	Fund.	Opt.	Fund.	Opt.	Fund.	Opt.	Fund.	Opt.	Fund.	Opt.	Fund.	Opt.	Fund.	Opt.
$Si_{29}H_{36}$	1.0	3.75	3.70	3.74	3.71	3.63	3.66	3.61	3.62	3.53	3.62	3.33	3.48	2.51	2.82	1.79	2.41
$Si_{87}H_{76}$	1.5	2.73	3.14	2.72	3.14	2.71	3.10	2.72	3.11	2.72	3.08	2.62	2.98	2.13	2.56	1.62	2.23
$Si_{175}H_{116}$	1.9	2.24	2.84	2.25	2.87	2.24	2.83	2.24	2.85	2.23	2.84	2.18	2.77	1.97	2.81	1.57	2.45
$Si_{389}H_{196}$	2.5	1.80	2.70	1.80	2.70	1.80	2.70	1.80	2.70	1.80	2.70	1.76	2.66	1.79	2.65	1.56	2.29
$Si_{705}H_{300}$	3.0	1.51	2.59	1.51	2.60	1.51	2.59	1.51	2.59	1.51	2.59	1.51	2.60	1.50	2.56	1.42	2.53
$Si_{1087}H_{412}$	3.5	1.35	2.56	1.35	2.57	1.35	2.57	1.35	2.57	1.35	2.57	1.35	2.57	1.34	2.55	1.29	2.54

[a]The number of hydrogen atoms refers to fully hydrogenated Si NCs. Note that in the NC models every Si atom with only one Si neighbor was replaced by hydrogen; for more details, see Ref. [3].

calculated HOMO-LUMO gaps are in good agreement with other theoretical calculations for Si NCs with different surface impurities; see Fig. 7.

The most noticeable feature in Fig. 6 is the different effect that the −O−, SB, and DB impurities have on both the HOMO-LUMO gap and the optical absorption gap. Both gaps in the NCs with SB impurities closely follow the gaps in the hydrogenated NCs, getting lower as the NCs size grows. Furthermore, with increasing NC size, the difference between the HOMO-LUMO gap and the optical absorption gap gets larger, regardless of the SB impurity. The only small difference, between the hydrogenated NC and the NCs with surface impurities, appears for the 1.0-nm NCs, where both gaps of the NCs with surface impurities are slightly lower than the gaps in the hydrogenated NC. The −O− has greater influence on both gaps, compared to the SB impurities, lowering the gaps even for the bigger NCs, showing a slight difference with the fully hydrogenated NCs up to 2.5 nm in size.

Contrary to the SB impurities, the DB impurities induce significant changes in the HOMO-LUMO and optical absorption gaps, with increasing NC size. The effect of the DB impurities is especially noticeable for the smaller NCs, where both gaps are considerably lowered compared to the gaps in the hydrogenated NCs. A similar behavior of the gaps in NCs with increasing size was previously reported for NCs with =O on the surface [32–34,54]. However, the dependence on the size of the NCs of both gaps is rather different. The HOMO-LUMO gaps, on one hand, are decreasing with increasing NC size, eventually becoming close to the gaps in the hydrogenated NCs. On the other hand, the optical absorption gaps first become smaller, then increase, and later get close to the gaps in the hydrogenated NCs. This unusual behavior of the optical absorption gaps comes from the changes in the origin of the states around the gap, when the NC size is increased.

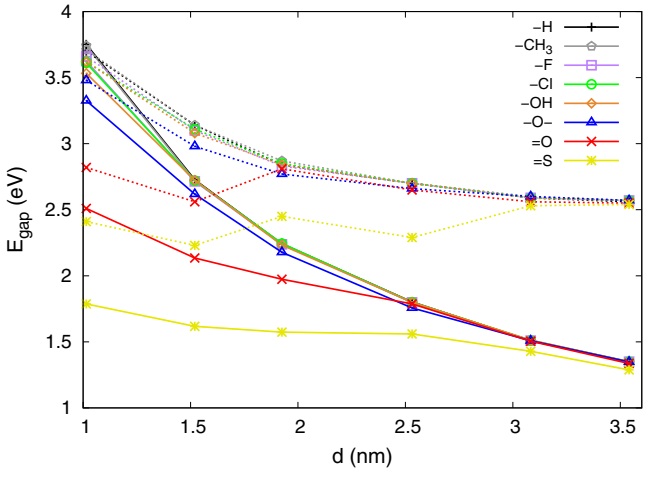

FIG. 6. (Color online) HOMO-LUMO gaps (solid lines) and optical absorption gaps (dotted lines) for Si NCs with different impurities. The gaps of NCs with $-CH_3$, −F, −Cl, −OH, −O−, =O, and =S impurities are shown in gray, purple, green, orange, blue, red, and yellow, respectively. The gaps of the fully hydrogenated NC (−H) are shown in black.

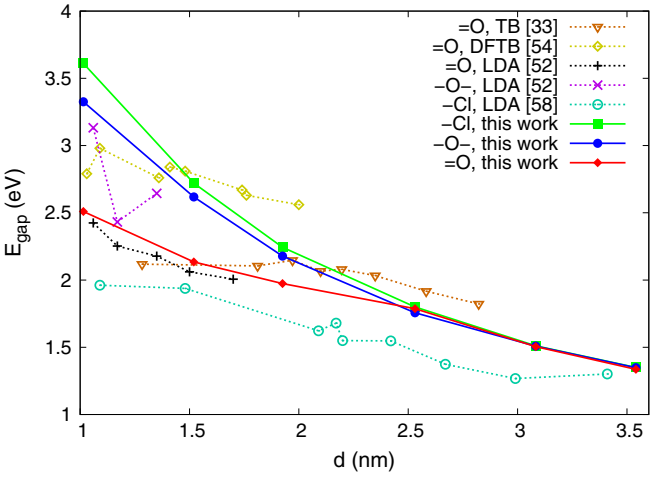

FIG. 7. (Color online) Comparison between the HOMO-LUMO gaps of Si NCs with −Cl (green), −O− (blue), and =O (red) impurities from the present work and the HOMO-LUMO gaps from other studies of Si NCs with (i) =O, calculated using tight-binding (TB) [33] (orange), DFT-LDA [52] (black) and density functional tight-binding (DFTB) [54] (yellow); (ii) −O−, calculated using DFT-LDA [52] (purple); and −Cl, calculated using DFT-LDA [55] (cyan).

The latter issue is discussed in more detail below, where the characteristics of the states around the gap are presented.

Moreover, we point out that for SB impurities and −O− the HOMO-LUMO and optical absorption gaps are approaching each other as the NCs size decreases. This follows the trend of transition from indirect band gap in bulk and large NCs to a direct band gap from small NCs [2–4]. In contrast, it is noticeable that the DB impurity induced a fairly large difference between the HOMO-LUMO gap and the optical absorption gap. Similar to the SB impurities, this difference in the gaps also grows as the size of the NCs with DB impurities increases, though it is less obvious compared to the other considered NCs. The effect of the =O impurity on both gaps is already reduced for the 2.0-nm NC, and both gaps are very close to the gaps of the hydrogenated 2.5-nm NC. Similar behavior of both gaps can be seen for the 3.1-nm NC with =S impurity, although the HOMO-LUMO gap is slightly lower than the gap in the hydrogenated 3.1-nm NC.

From the presented findings, concerning the effects of the −O−, SB, and DB impurities on the HOMO-LUMO and

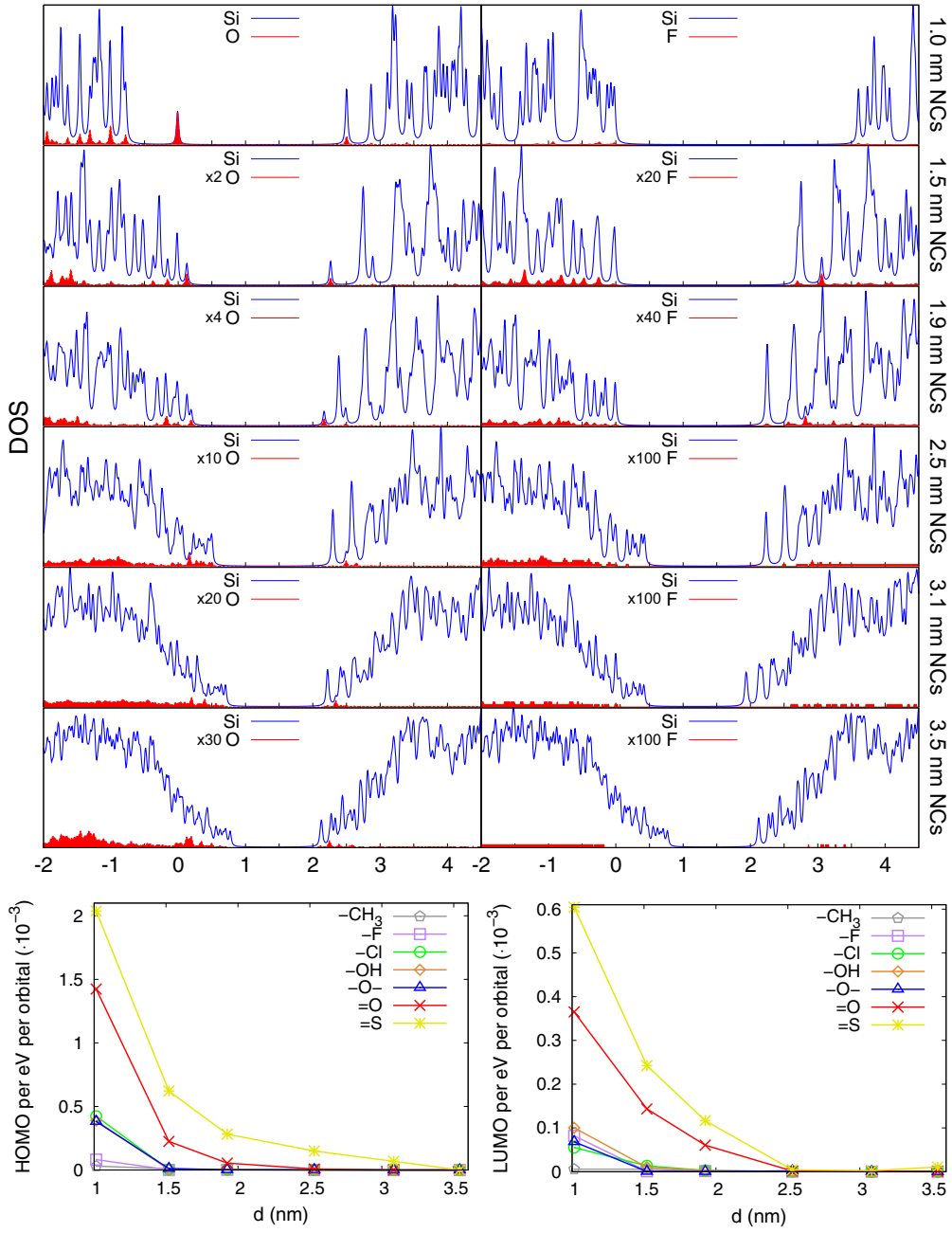

FIG. 8. (Color online) PDOS of Si NCs with different surface impurities and different size. The top panels show the PDOS of Si NCs with =O and −F impurity on the surface as a function of the size of the NCs. The PDOS of the impurity and the Si atoms are shown in red and blue, respectively. Note that the PDOS of the impurity, in structures bigger than 1.0 nm, are multiplied by a factor, given in the key, next to the impurity sign. The bottom left panel shows the integral over the HOMO state of the impurity as a function of the size of the NCs. The bottom right panel shows the integral over the LUMO state of the impurity as a function of the size of the NCs.

optical absorption gaps in the NCs with various sizes, there are a few points that need to be kept in mind. The effect of the impurity on both the HOMO-LUMO gap and the optical absorption gap, of the 1.0-nm NC is the biggest, regardless of the type of impurity. Already at the 1.5-nm NC, the change induced by the SB impurity becomes negligible. However, the DB impurity and −O− affects both gaps of the bigger NCs, with the difference becoming insignificant only for the 3.1-nm NC or larger. This shows that the NCs bigger than 3.1 nm are expected to perform similarly, despite the distinct impurities on the surface. This difference will increase as the size of the NCs decreases, being especially noticeable between the SB and DB impurities. Finally, not only the gaps, but also the DOS and absorption indices of the 1.0-nm NCs are the most susceptible to the changes of the surface impurities, following nearly the same trend as the HOMO-LUMO gaps.

V. HIGHEST OCCUPIED AND LOWEST UNOCCUPIED EIGENSTATES

To gain a better insight into how the surface impurity affects the HOMO-LUMO gap and the optical absorption gap, we investigated the contribution from the states of the impurity to the total DOS. Shown in Fig. 8 are the projected density of states (PDOS) of the impurity, compared to the PDOS of the Si atoms, for the NCs with =O and −F impurity. We have chosen these types of impurities because they are good representatives for the DB and SB impurities, respectively, as shown in the DOS and absorption indices. Moreover, oxygen is the most common surface impurity found on Si NCs, as discussed in the Introduction, and fluorine can be left as a residue when forming porous Si by HF etching of bulk Si. It is evident that the impurity states' contribution to the states around the gap decreases as the size of the NCs grows, regardless of the type of impurity. Furthermore, the contribution of the =O to the states around the gap in the NCs with same size is significantly larger compared to the contribution from the −F (note that the multiplication factor for the F states is an order of magnitude bigger than the one for O states).

To give a better overview for the changes in the contribution from the impurities, we calculated the integral over the HOMO and LUMO states for each of the studied structures; see the bottom two panels in Fig. 8. It is noticeable that the contribution to both the HOMO state and the LUMO state from the impurity decreases with increasing NC size in each of the studied impurities. The −O− and the SB impurities contribute to both states much less than the DB impurities, and their contribution becomes negligible for NCs bigger than 1.5 nm. The DB impurities, on the other hand, have a rather high contribution for NCs with size up to 2.5 nm, with the contribution from the =S impurity to the HOMO state extending to the bigger NC. It is also interesting to notice the fairly minor contribution from the =O to both HOMO and LUMO states for structures bigger than 2.5 nm. This is in agreement with Vasiliev *et al.* [34], who predicted that the contribution from the O states to the HOMO and LUMO states should disappear for structures bigger than 2–2.5 nm.

To illustrate in more detail how the states around the gap are changing with increasing NC size, and to make a comparison with the the hydrogenated Si NCs [3], we

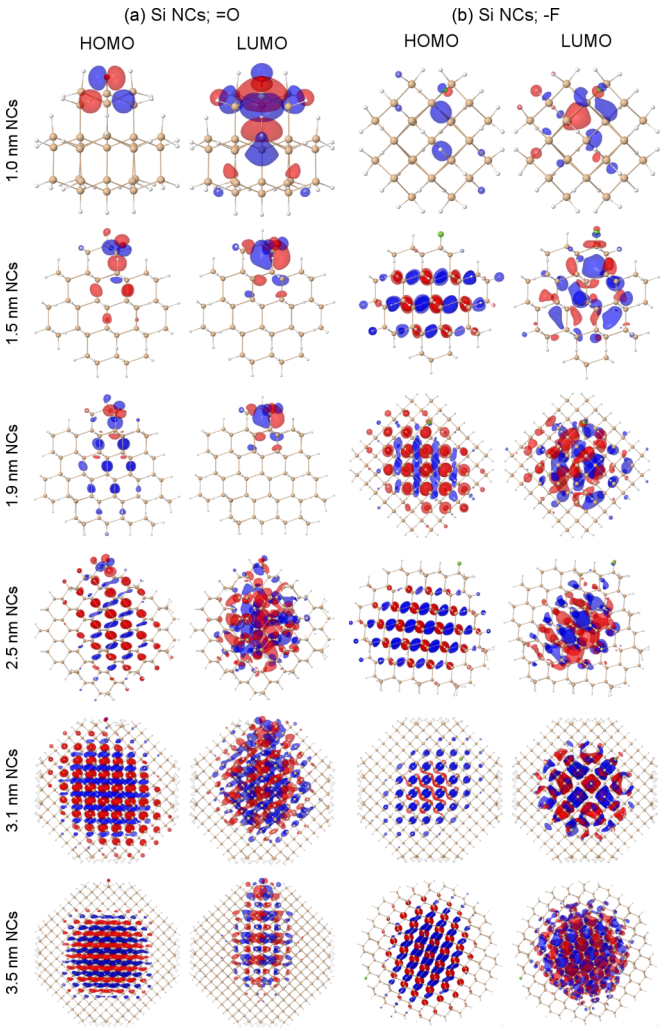

FIG. 9. (Color online) Size dependence of the HOMO and LUMO WFs for Si NCs with (a) =O and (b) −F impurity. The O, F, Si, and H atoms are shown in red, green, tan, and white, respectively. The isosurfaces for each of the NCs with =O and −F are respectively chosen at 10% and 40% of the maximum.

calculated the HOMO and LUMO WFs for the NCs with =O and −F impurity; see Fig. 9. The most noticeable result is the considerable influence of the =O on the HOMO and LUMO state, of the NCs lower than 1.9 nm. Both the HOMO and the LUMO WFs exhibit significant localization around the O atom, with the LUMO WF being affected more by the impurity. With increasing NC size, both WFs are becoming more delocalized, spreading more into the core of the NCs. It is also worth noticing that even in the biggest NC, 3.5 nm, the LUMO WF has non-negligible localization at the O atom. This is a very interesting observation, which is not evident from the PDOS, where an insignificant contribution from the O atom in the LUMO state is seen (see Fig. 8). In the case of the Si NCs with −F impurity, the HOMO and LUMO WFs for the 1.0-nm NC are mainly localized around the F atom. The delocalization of both WFs increases with growing NC size, with the WFs spreading more into the core of the NC. Similarly to the NCs with =O impurity, the LUMO WFs of the NCs with −F impurity are influenced more by the impurity, compared

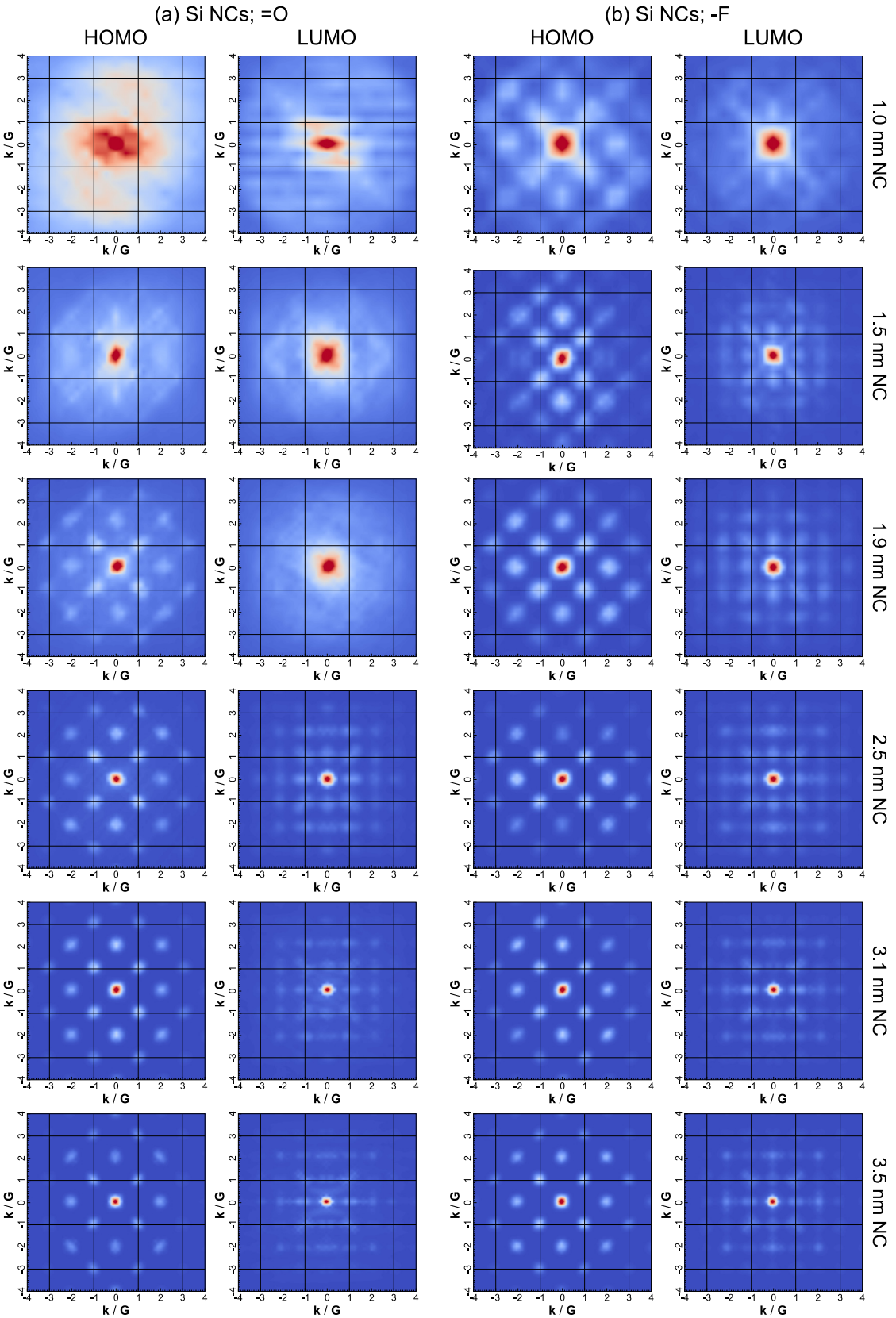

FIG. 10. (Color online) Fourier transform of the HOMO and LUMO charge density of Si NCs with (a) =O and (b) −F impurity, as a function of the size of the NCs. The Fourier transform of the HOMO charge densities are shown in the left column of each panel, and the LUMO charge density in the right column of each panel. The Fourier transform is an average of the projections on x-y, x-z, and y-z planes. The red color maps the highest values and the blue color the lowest value of the charge densities within a fixed range for all sizes (in arbitrary units). The **k** is scaled by the reciprocal vector **G** of size $\frac{2\pi}{a}$.

to the HOMO WFs, though the delocalization and shift of HOMO and LUMO from surface impurity to the core begin at smaller size for −F impurity and appear to be complete for NCs larger than 3 nm.

Although in the real space, the localization of the WFs is clearly visualized, the Fourier transform (FT) of the charge densities gives a complementary angle of view and additional insight into the changes in both the localization and the symmetry of the HOMO and LUMO states. Ultimately, changes in both of these features will affect the properties of the Si NCs with changes in the surface impurities and the NC size. Therefore, we calculated the FT of the HOMO and LUMO charge densities for the NCs with =O and −F impurity. Because the orientation of the various impurities on the surface of the NCs differs from each other, choosing a particular plane on which the 3D FT is being projected can be biased. Hence, we calculated an average of the projection of the 3D FT on the x-y, x-z, and y-z planes, and the resulting averages are shown on Fig. 10.

Similarly to the WFs in real space, in the FT of the charge densities there is also noticeable influence of the =O on the HOMO and LUMO states. The FT of both HOMO and LUMO states is rather delocalized, suggesting that there is a significant localization of the charge density and indicating no apparent periodicity within the NC, as seen from the WFs in real space (see Fig. 9). However, the FT of the HOMO charge density of the 1.9-nm NCs has some distinct spots, indicating that the WF is spread across the core of the NC and is very different from the FT of the LUMO charge density, which shows a rather high delocalization in k space. Similarly, using a tight-binding method, Wolkin *et al.* [33] have shown that, depending on the NCs size, the hole and electron states in Si NCs with one =O impurity on the surface become closer to the respective states in hydrogenated NCs. They show that the hole states are closing up already in ∼1.5 nm NCs and, on the other hand, the electron states are becoming close for larger NCs, ∼2.9 nm.

As the size of the NCs is growing beyond 1.9 nm, the influence of the =O becomes negligible, and the FT of the charge densities reveals higher periodicity of the states in the NCs, shown by higher number of spots in the FT. This increased periodicity suggests that the WFs are delocalized in the core of the NCs, which is also observed for the WFs in real space (see Fig. 9). Moreover, the FT of the HOMO and LUMO charge densities for the NCs with =O is very similar to the FT of the NCs with −F for the NCs bigger than 1.9 nm. For the smaller NCs with −F, the FT of the charge densities shows some periodicity, except for the 1.0-nm NC, where the delocalization of the FT is the highest, seen as an increased localization in the real space (see Fig. 9). Increased number of spots in the FT of the HOMO and LUMO charge densities with growing NC size is also observed for hydrogenated Si NCs [3].

The increased contribution from the impurities to the states around the gap will influence the symmetry of the states, as seen from the top three rows in Fig. 10, causing the transitions from the unoccupied to the occupied states to be more probable. This, in turn, will increase the optical response, giving rise to additional peaks in the gap region of the absorption indices. These peaks are almost nonexistent in the larger NCs (see Fig. 5), where the contribution from the impurity to the states around the gap is significantly low. However, as the size of the NCs is reduced, this contribution increases, manifesting itself with an increased number of small peaks in the absorption indices. This is particularly noticeable for the smaller NCs with DB impurities, where the peaks become more intense as the size of the NCs deceases [see Fig. 5(g)].

VI. CONCLUSIONS

We have presented a detailed first-principles, ground-state DFT study of the evolution of the electronic and optical properties of Si NCs, with surface impurities, as a function of NC size. We show that the DOS and absorption indices of NCs with SB impurities ($-CH_3$, −F, −Cl, −OH) and bridged oxygen (−O−) are very similar to the properties of the hydrogenated NCs, except for the 1.0-nm NCs showing slightly different properties. Unlike the NCs with SB impurities, the NCs with DB impurities (=O, =S) show significant differences in the DOS and absorption indices, compared to the respective properties of hydrogenated NCs. This difference is especially noticeable for the smaller NCs, with size less than 2.5 nm, where the states in the gap region appear. Furthermore, we show that the HOMO-LUMO and optical absorption gaps of the NCs with SB impurities follow the same trend as the gaps in the hydrogenated NCs. However, both gaps, in the NCs with DB impurities and bridged oxygen, are very different from the gaps in the hydrogenated NCs, showing significant difference for NCs smaller than 2.5 nm.

We argue that this difference in both gaps arises from the different contribution from the states of the impurity atom to the states around the gap. This is especially noticeable for the smaller NCs, where the contribution of the states of the impurity is the highest. Moreover, we show that the states of the impurity are shifted towards the body of the NCs, as the size of the NCs are growing. We further support this finding by demonstrating that the real part and the FT of the HOMO and LUMO charge densities, for the smaller NCs, indicate a significant localization of the charge densities around the impurity. We argue that this observation, together with the insignificant contribution from the states of the DB impurity, are the main factors for the very small difference in HOMO-LUMO and optical absorption gaps of the NCs bigger than 2.5 nm. Finally, we show that the stability of the smallest NCs depends substantially on the impurity and becomes rather similar with increasing NC size. In addition, we demonstrate that high hydrogen concentration is needed to give the hydrogenated Si NCs higher stability than that of Si NC with oxygen or fluorine impurity. A high H_2 concentration is required even at very low concentrations of oxygen.

ACKNOWLEDGMENTS

This work was supported by the EU's 7th Framework Programme SNAPSUN. J.R. and O.E. acknowledge the support of Swedish Research Council. O.E. also acknowledges support from the Knut and Alice Wallenbergs foundation and the European Research Council (Project No. 247062-ASD), as well as eSSENCE and STANDUPP.

[1] L. T. Canham, Appl. Phys. Lett. **57**, 1046 (1990).
[2] F. Trani, G. Cantele, D. Ninno, and G. Iadonisi, Phys. Rev. B **72**, 075423 (2005).
[3] V. Kocevski, O. Eriksson, and J. Rusz, Phys. Rev. B **87**, 245401 (2013).
[4] P. Hapala, K. Kůsová, I. Pelant, and P. Jelínek, Phys. Rev. B **87**, 195420 (2013).
[5] L. Pavesi, L. Dal Negro, C. Mazzoleni, G. Franzò, and F. Priolo, Nature (London) **408**, 440 (2000).
[6] R. Anthony and U. Kortshagen, Phys. Rev. B **80**, 115407 (2009).
[7] D. Timmerman, J. Valenta, K. Dohnalová, W. D. A. M. de Boer, T. Gregorkiewicz, Nat. Nanotechnol. **6**, 710 (2011).
[8] J. R. Rodrguez, J. G. C. Veinot, P. Bianucci, and A. Meldrum, Appl. Phys. Lett. **92**, 131119 (2008).
[9] M. Ghulinyan, D. Navarro-Urrios, A. Pitanti, A. Lui, G. Pucker, and L. Pavesi, Opt. Express **16**, 13218 (2008).
[10] K. D. Hirschman, L. Tsybeskov, S. P. Duttagupta, and P. M. Fauchet, Nature (London) **384**, 338 (1996).
[11] R. J. Walters, G. I. Bourianoff, and H. A. Atwater, Nat. Mater. **4**, 143 (2005).
[12] K.-Y. Cheng, R. Anthony, U. R. Kortshagen, and R. J. Holmes, Nano Lett. **11**, 1952 (2011).
[13] F. Maier-Flaig, J. Rinck, M. Stephan, T. Bocksrocker, M. Bruns, C. Kübel, A. K. Powell, G. A. Ozin, and U. Lemmer, Nano Lett. **13**, 475 (2013).
[14] E. H. Sargent, Adv. Mater. **17**, 515 (2005).
[15] N. Daldosso and L. Pavesi, Laser Photon. Rev. **3**, 508 (2009).
[16] K.-Y. Cheng, R. Anthony, U. R. Kortshagen, and R. J. Holmes, Nano Lett. **10**, 1154 (2010).
[17] S. Chan, Y. Lib, L. J. Rothbergb, B. L. Millerb, P. M. Faucheta, Mater. Sci. Eng., C **15**, 277 (2001).
[18] E. A. Konstantinova, L. A. Osminkina, K. S. Sharov, E. V. Kurepina, P. K. Kashkarov, V. Yu. Timoshenko, J. Exp. Theor. Phys. **99**, 741 (2004).
[19] L. Rebohle, T. Gebel, R. A. Yankov, T. Trautmann, W. Skorupa, J. Sun, G. Gauglitz, and R. Frank, Opt. Mater. **27**, 1055 (2005).
[20] C. M. Gonzalez, M. Iqbal, M. Dasog, D. G. Piercey, R. Lockwood, T. M. Klapotke, and J. G. C. Veinot, Nanoscale **6**, 2608 (2014).
[21] Y. Feng, Y. Liu, C. Su, X. Ji, and Z. He, Sens. Actuators, B **203**, 795 (2014).
[22] V. Švrček, A. Slaoui, and J.-C. Muller, Thin Solid Films **451-452**, 384 (2004).
[23] G. Conibeer, M. Green, R. Corkish, Y. Cho, E.-C. Cho, C.-W. Jiang, T. Fangsuwannarak, E. Pink, Y. Huang, T. Puzzer, T. Trupke, B. Richards, A. Shalav, and K.-L. Lin, Thin Solid Films **511**, 654 (2006).
[24] D. Song, E.-C. Cho, G. Conibeer, C. Flynn, Y. Huang, and M. A. Green, Sol. Energy Mater. Sol. Cells **92**, 474 (2008).
[25] M. Govoni, I. Marri, and S. Ossicini, Nat. Photonics **6**, 672 (2012).
[26] Z. F. Li and E. Ruckenstein, Nano Lett. **4**, 1463 (2004).
[27] J. H. Warner, A. Hoshino, K. Yamamoto, and R. D. Tilley, Angew. Chem. Int. Ed. **44**, 4550 (2005).
[28] F. Erogbogbo, K.-T. Yong, I. Roy, G. Xu, P. N. Prasad, and M. T. Swihart, ACS Nano **2**, 873 (2008).
[29] J. Park, L. Gu, G. von Maltzahn, E. Ruoslahti, S. N. Bhatia, and M. J. Sailor, Nat. Mater. **8**, 331 (2009).
[30] E. Borsellaa, R. DAmatoa, M. Falconieria, E. Travea, A. Panaritia, and I. Rivolta, J. Mater. Res. **28**, 193 (2013).
[31] Y. Zhong, F. Peng, F. Bao, S. Wang, X. Ji, L. Yang, Y. Su, S.-T. Lee, and Y. He, J. Am. Chem. Soc. **135**, 8350 (2013).
[32] A. Puzder, A. J. Williamson, J. C. Grossman, and G. Galli, Phys. Rev. Lett. **88**, 097401 (2002).
[33] M. V. Wolkin, J. Jorne, P. M. Fauchet, G. Allan, and C. Delerue, Phys. Rev. Lett. **82**, 197 (1999).
[34] I. Vasiliev, J. R. Chelikowsky, and R. M. Martin, Phys. Rev. B **65**, 121302(R) (2002).
[35] L. E. Ramos, J. Furthmüller, and F. Bechstedt, Phys. Rev. B **70**, 033311 (2004).
[36] M. Luppi and S. Ossicini, Mater. Sci. Eng. B **101**, 34 (2003).
[37] L. E. Ramos, J. Furthmüller, and F. Bechstedt, Appl. Phys. Lett. **87**, 143113 (2005).
[38] M. S. Brandt, H. D. Fuchs, M. Stutzmann, J. Weber, and M. Cardona, Solid State Commun. **81**, 307 (1992).
[39] S. Schuppler, S. L. Friedman, M. A. Marcus, D. L. Adler, Y.-H. Xie, F. M. Ross, T. D. Harris, W. L. Brown, Y. J. Chabal, L. E. Brus, and P. H. Citrin, Phys. Rev. Lett. **72**, 2648 (1994).
[40] J. von Behrena, T. van Buurenb, M. Zachariasc, E. H. Chimowitzd, and P. M. Fauchete, Solid State Commun. **105**, 317 (1998).
[41] T. van Buuren, L. N. Dinh, L. L. Chase, W. J. Siekhaus, and L. J. Terminello, Phys. Rev. Lett. **80**, 3803 (1998).
[42] D. S. English, L. E. Peli, Z. Yu, P. F. Barbara, and B. A. Korgel, Nano Lett. **2**, 681 (2002).
[43] J. H. Warner, H. Rubinsztein-Dunlop, and R. D. Tilley, J. Phys. Chem. Lett. **109**, 19064 (2005).
[44] C. Delerue, G. Allan, and M. Lannoo, Phys. Rev. B **48**, 11024 (1993).
[45] L.-W. Wang and A. Zunger, Phys. Rev. Lett. **73**, 1039 (1994).
[46] S. Öğüt, J. R. Chelikowsky, and S. G. Louie, Phys. Rev. Lett. **79**, 1770 (1997).
[47] M. Rohlfing and S. G. Louie, Phys. Rev. Lett. **80**, 3320 (1998).
[48] L. X. Benedict, A. Puzder, A. J. Williamson, J. C. Grossman, G. Galli, J. E. Klepeis, J.-Y. Raty, and O. Pankratov, Phys. Rev. B **68**, 085310 (2003).
[49] L. E. Ramos, J. Paier, G. Kresse, and F. Bechstedt, Phys. Rev. B **78**, 195423 (2008).
[50] D. Neuhauser, Y. Gao, C. Arntsen, C. Karshenas, E. Rabani, and R. Baer, Phys. Rev. Lett. **113**, 076402 (2014).
[51] I. Vasiliev, S. Öğüt, and J. R. Chelikowsky, Phys. Rev. Lett. **86**, 1813 (2001).
[52] A. Puzder, A. J. Williamson, J. C. Grossman, and G. Galli, J. Chem. Phys. **117**, 6721 (2002).
[53] C. S. Garoufalis and A. D. Zdetsis, Phys. Chem. Chem. Phys. **8**, 808 (2006).
[54] Q. S. Li, R. Q. Zhang, and S. T. Lee, Appl. Phys. Lett. **91**, 043106 (2007).
[55] A. Carvalho, S. Öberg, M. J. Rayson, P. R. Briddon, Phys. Rev. B **86**, 045308 (2012).
[56] E. Ramos, B. M. Monroy, J. C. Alonso, L. E. Sansores, R. Salcedo, and A. Martínez, J. Phys. Chem. C **116**, 3988 (2012).
[57] M. Luppi and S. Ossicini, J. Appl. Phys. **94**, 2130 (2003).
[58] F. A. Reboredo and G. Galli, J. Phys. Chem. B **109**, 1072 (2005).
[59] P. Ordejón, E. Artacho, and J. M. Soler, Phys. Rev. B **53**, R10441 (1996); J. M. Soler, E. Artacho, J. D. Gale, A. García, J. Junquera, P. Ordejón, and D. Sánchez-Portal, J. Phys. Condens. Matter **14**, 2745 (2002).

[60] E. Degoli, S. Ossicini, G. Cantele, E. Luppi, R. Magri, D. Ninno, O. Bisi1, Phys. Status Solidi C **2**, 3354 (2005).

[61] X. Chen, X. Pi, and D. Yang, J. Phys. Chem. C **114**, 8774 (2010).

[62] The energies of O, Cl, and F correspond to the calculated energy per atom for O_2, Cl_2, and F_2 molecules, respectively. The energy of S is taken from the calculated energy per atom of bulk S. The energy of CH_3 is calculated as a difference between the calculated energy of CH_4 molecule and the energy per atom of H_2. The energy of OH is calculated as a difference between the energy of an H_2O molecule and the energy per atom of H_2.

[63] M. W. Chase, Jr., *NIST-JANAF Thermochemical Tables*, 4th Edition, Monograph No. 9, Journal of Physical and Chemical Reference Data, (1998), p. 1051, 1261, 1717.

[64] A. Zunger and A. J. Freeman, Phys. Rev. B **17**, 4850 (1978); A. E. Carlsson, *ibid.* **31**, 5178 (1985).

[65] H.-Ch. Weissker, J. Furthmüller, and F. Bechstedt, Phys. Rev. B **65**, 155328 (2002).

[66] C. Delerue, M. Lannoo, and G. Allan, Phys. Rev. Lett. **84**, 2457 (2000).

[67] A. J. Williamson, J. C. Grossman, R. Q. Hood, A. Puzder, and G. Galli, Phys. Rev. Lett. **89**, 196803 (2002).